Proceedings of the 6th International Conference on the Application of Physical Modelling in Coastal and Port Engineering and Science (Coastlab16)

Ottawa, Canada, May 10-13, 2016

EXPERIMENTAL INVESTIGATION OF HYDRODYNAMIC CHARACTERISTICS OF TWIN CIRCULAR SUBMERGED FLOATING TUNNEL

SANG-HO OH[1], WOO SUN PARK[2]

1 Korea Institute of Ocean Science and Technology, Republic of Korea, coast.oh@gmail.com

2 Korea Institute of Ocean Science and Technology, Republic of Korea, wspark@kiost.ac.kr

ABSTRACT

A submerged floating tunnel (SFT) is a unique marine structure that has not been actually constructed till date. An assessment of the hydrodynamic performance of an SFT under wave loading is important when designing an SFT structure. In this study, experiments were conducted in a two-dimensional wave flume to investigate the hydrodynamic characteristics of a twin circular SFT model under the action of regular waves having different heights and periods. Three different configurations of the twin SFT model were tested in the experiment. The experimental results showed that the three-degree motions of the twin SFT and the associated tensile forces acting on the tension legs vary considerably according to the change in the configurations of the model. All the configurations considered in this study were found to be inadequate in satisfactorily restricting the horizontal and vertical motions of the SFT model.

KEWORDS: Submerged floating tunnel, Wave force, Hydrodynamic response, Tension leg, Physical experiment

1 INTRODUCTION

A submerged floating tunnel (SFT) is a unique marine structure whose hydrodynamic stability is maintained by the balance between the buoyancy and tethering of the structure (Jakobsen, 2010). An SFT is a fascinating solution for connecting two shore areas that are separated by a narrow and deep sea strait, lake, or river, where it is very hard to build a conventional tunnel or bridge across the shores. The concept of this structure was introduced several decades ago, but a prototype SFT has not yet been constructed anywhere in the world.

The actual realization of an SFT requires many considerations regarding its design, such as structural shape and tethering methods. Fundamental data for the design of an SFT include the hydrodynamic loads driven by a wave, current, earthquake, and tsunami. Some research has been conducted in order to assess the hydrodynamic performance of an SFT against these loads (Hong and Ge, 2010; Jakobsen, 2010; Kunish, 2010; Lu et al., 2011; Dong et al., 2012; and others).

All previous researches focused on the characteristics of a single SFT structure. If we consider the practical application of the structure in the field, a twin SFT can be an optional design depending on requirements under certain conditions. Therefore, physical experiments were carried out in a two-dimensional wave flume to examine the hydrodynamic characteristics of a twin SFT having different link configurations. By varying the conditions of wave heights and periods, the hydrodynamic behavior of the SFT model and the tensile forces acting on the tension legs were quantitatively assessed in this study.

2 PHYSICAL EXPERIMENTS

The experiments were conducted in a two-dimensional wave flume with a length, height, and width of 53, 1.25, and 1 m, respectively. The SFT model was manufactured using acrylic plastic and was sealed to prevent the penetration of water into it. The cross-section of the model was a circle with a diameter of 23 cm. The length of the model was 98 cm, or 2 cm less than the width of the wave flume. The SFT model did not hit on the side walls of the flume because the motion of the SFT was intrinsically two-dimensional. Considering the SFT structure that can be realized in the field, the scale of the model in the experiment is assumed to be approximately 1/100 of an actual prototype structure.

Three different configurations were tested in the experiment. The configurations differed by the link between the twin circular SFT models as shown in Figures 1 and 2. As shown in the figures, the movement of each SFT model was restricted

by tension legs that were fixed to the floor of the flume. The ends of the tension legs were connected to load cells mounted on the bottom of the flume. As shown in Figure 3, eight load cells were used to measure the tensile force acting on the tension legs. Stainless steel wire AISI304 was used as the material for the tension legs, which have an elastic modulus of 197 GPa. The distance between the neighboring tension legs in the transverse direction was 50 cm in the experiment.

The SFT model was installed in such a manner that its top point is located 50 cm above the floor of the flume. Because the water depth was fixed at 80 cm, the corresponding clearance of the model was 30 cm. A buoyancy to weight ratio (BWR) of 1.3 was adopted in the experiment. Under this BWR condition, the initial tension acting on a single tension leg was 61.4 N for all three configurations. The SFT model was securely sealed to prevent the infiltration of water during the experiment. Regular waves having 16 different wave heights and periods were generated for 60 s to measure the hydrodynamic characteristics of the twin SFT model. The values of wave heights differ depending on the wave periods and the wave steepness, as indicated in Table 1, which summarizes the conditions of the test waves and experimental setup.

The wave loading on the structure due to the wave action was measured using eight pressure gauges attached around the central cross-section of the model. The conceptual diagram showing the arrangement of the pressure gauges is provided in Figure 4. In addition, the movement of the SFT model was assessed by taking a video during the experiments and analyzing the video using image processing techniques. The dynamic response of the model structure against the wave load was accurately estimated by calculating the relative displacement of two black circle markers attached on the glass side of the SFT model.

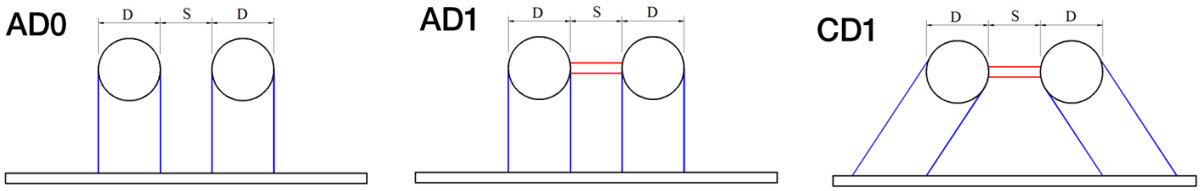

Figure 1. Conceptual diagram of the three different configurations of the twin SFT.

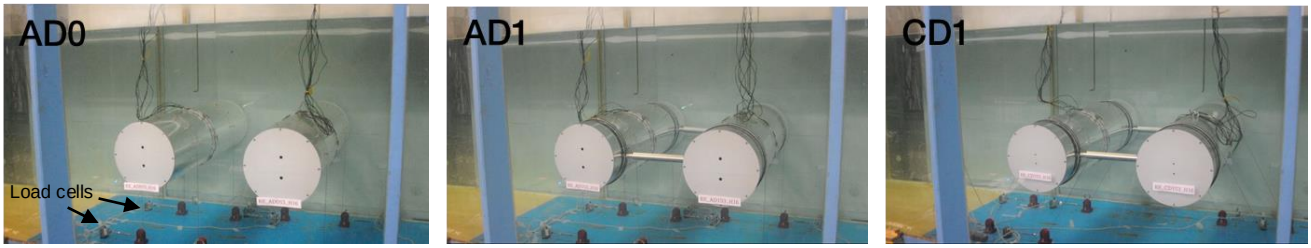

Figure 2. Three different configurations of the twin SFT model installed in the wave flume

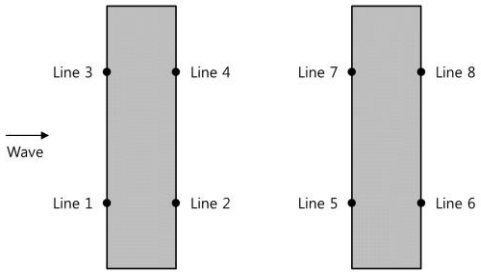

Figure 3. Plan view of the twin SFT with notations of the tension legs.

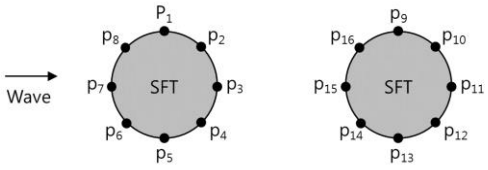

Figure 4. Side view of the twin SFT with notations of the pressure gauges.

Table 1. Summary of the experimental conditions.

Quantity	Values	Unit
Diameter of the tunnel model, *D*	23	[cm]
Water depth, *h*	0.8	[cm]
Buoyancy–Weight Ratio (BWR)	1.3	[-]
Wave period, *T*	0.65, 0.8, 1.0, 1.3	[s]
Wave steepness, *s*	0.013, 0.027, 0.040, 0.053	[-]
Wave height, *H*	0.85–13.0	[cm]

3 EXPERIMENTAL RESULTS

The displacement and rotation of the SFT model was calculated by applying image processing techniques to the acquired video clips that monitor the movement of two markers attached on the side of the model. The acquired images were first transformed into binary images, and the location of the two markers were detected. Then, the displacement and rotation of the model can be easily calculated.

Figure 5 shows the maximum and minimum values of sway (horizontal) motion of the twin SFT model for the three configurations when T = 1.3 s. It was found that the sway motions increased almost linearly with the wave height. In addition, the magnitudes of maximum and minimum sway were similar as the SFT model moved back and forth periodically under wave action. Among the three configurations, the CD1configuration showed the least sway motion. The sway motions of the AD0 and AD1configurations were comparatively large because the tension legs hold the SFT model only in the vertical direction, which results in a relatively large horizontal displacement of the model. A comparison of the sway of the first and second tunnel showed that the magnitude of the sway of the second tunnel is slightly smaller as it is influenced by the sway motion of the the first tunnel.

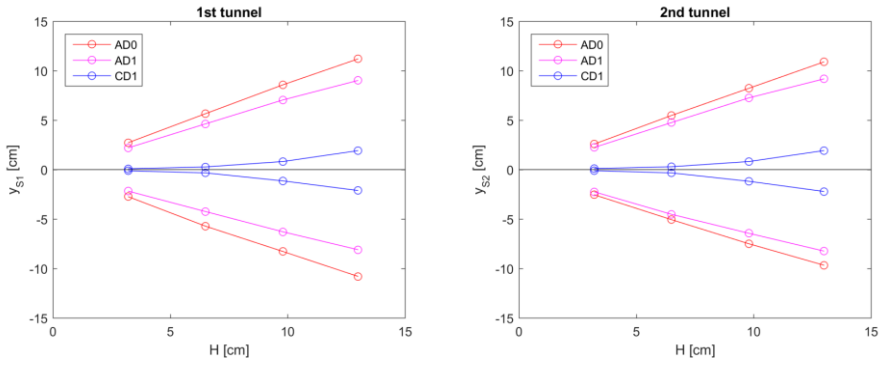

Figure 5. Sway motions of the twin SFT model (*T* = 1.3 s).

The magnitudes of the pitch (vertical) motions were significantly smaller than those of the sway motions, as shown in Figure 6. In particular, the positive pitch motions were nearly zero for the AD0 and AD1 configurations because the upward movement of the SFT model is restricted by the tension legs. However, recognizable positive pitch motions were observed in the CD1 configuration owing to the occurrence of slight distortion in the SFT models. The negative pitch motions showed a monotonously increasing trend with the wave height. Such a trend was observed owing to the increase in the sway motions

with the wave height, as shown in Figure 5. The AD0 configuration had the largest negative pitch among the three configurations because the sway motions were the largest with the AD0 configuration. Similar to the sway motion, the pitch motions of the second SFT model were slightly smaller than those of the first SFT model.

The results for the roll motions of the twin SFT model are shown in Figure 6. In case of the AD0 and AD1 configurations, the maximum and minimum magnitudes of the roll motions were almost comparable, whereas those of the CD1 configuration were not. Such behavior was a result of the significant torsion of the twin SFT models in the CD1 configuration, especially when the wave height was relatively large. The distortion of the SFT models in the CD1 configuration occurred because the two models were connected to each other by a horizontal bar, and the horizontal movement of the models were not perfectly restricted by the obliquely installed tension legs; the movement was in fact not very well restricted. When the models were subjected to significant horizontal loading by waves, each model was likely to rotate in a different direction, resulting in the distortion of the SFT models.

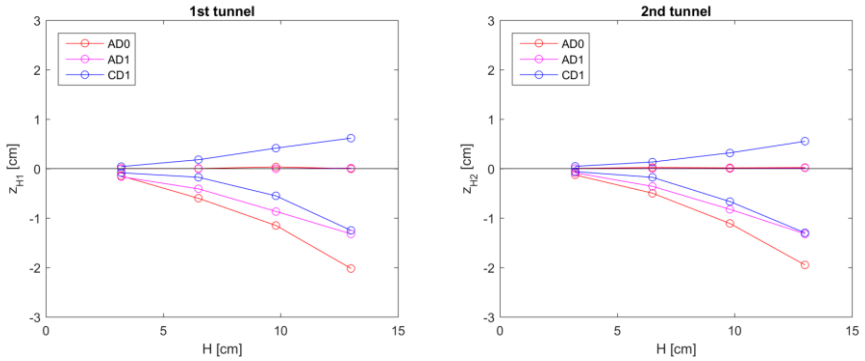

Figure 6. Pitch motions of the twin SFT model (T = 1.3 s).

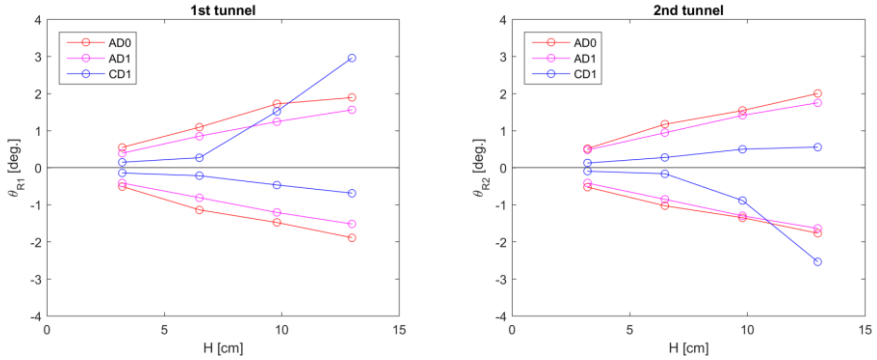

Figure 7. Roll motions of the twin SFT model (T = 1.3 s).

Next, the dynamic tensile forces acting on the four tension legs holding the SFT models were examined by analyzing the measured data from the load cells connected to the tension legs. Figure 8 shows the maximum tensile forces acting on the tension legs for the AD0 configuration when T = 1.3 s. In the figure, F_{T1} denotes the mean tensile force of Lines 1 and 2 shown in Figure 3. Similarly, F_{T2} is the mean value of Lines 3 and 4. For the second SFT, F_{T3} and F_{T4} represent the mean tensile forces of Lines 5 and 6 and Lines 7 and 8, respectively. Figure 8 shows the dynamic tensile forces under wave action, so the magnitude of the initial tension has no effect on the results. In general, the maximum tensile forces acting on the tension legs linearly increased with the wave height. The maximum and minimum tensile forces on F_{T1} and F_{T2} were similar, indicating that there was little imbalanced motion of the first SFT model in the transverse direction across the wave flume. The maximum and minimum values of F_{T3} and F_{T4} were also in good agreement with each other, confirming the two-dimensional behavior of the second SFT model either.

When the tensile forces acting on the first and second SFT models are compared in Figure 8, both the maximum and minimum values of the second model are lower than those of the first model. However, the magnitudes of the maximum forces are almost comparable to each other, whereas a clear difference is observed between the minimum forces of the two SFT models. Such a difference can be attributed to the wave action on the second model being reduced owing to the blockage effect of the first model. Although the behavioral difference in the sway or pitch motions between the first and second model shown in Figures 5 and 6 was not as large as in Figure 8, a slight reduction in the overall movement of the model may lead to a significant reduction in the tensile force. In particular, when the maximally stretched tension leg turns back to shrink, the

amount of tension loss from the maximum tensile force may differ depending on each of the tension legs. The maximum tensile force acting on the first SFT model was 27.0 N, which implies that the dynamic tensile force was approximately 44% of the initial tension in the AD0 configuration.

The tensile forces acting on the tension legs in the AD1 configuration is shown in Figure 9. In this case, the maximum and minimum forces of F_{T1} and F_{T2} on the first SFT model showed a significant discrepancy, whereas those of F_{T3} and F_{T4} on the second model were generally similar. Another difference from the previous case (AD0) is that the minimum values of F_{T1} and F_{T2} did not decrease monotonously with the wave height. As shown in the figure, the minimum tensile force when H = 13 cm was greater than that when H = 9.8 cm. The reason for these phenomena is not clear, but it can be ascribed to the two metallic bars that horizontally connect the two SFT models because the only difference between the AD0 and AD1 configurations is the additional placement of the bars. The presence of the bars meant that the twin SFT models had to move together, preventing independent displacement of each model. This was found to be helpful in reducing the sway, pitch, and roll motions of the two SFTs, as shown in Figures 5 to 7. At the same time, however, unnatural imbalance of the tensile forces acting on the tension legs occurs, as shown in Figure 9.

Figure 10 shows the results for the tensile forces in the CD1 configuration. In this case, the magnitudes of the maximum tensile forces were more than four times those of the corresponding values in the AD1 configuration. As shown in Figures 1 and 2, the only difference between the AD1 and CD1 configurations is the angle at which the tension legs hold the SFT models. The tension legs were vertical in the AD1 configuration, whereas they were inclined at 45° in the CD1 configuration. It was found that the CD1 configuration has an advantage in restricting the horizontal movement of the SFT models because the sway motion is significantly smaller than the sway motion in the ADI configuration, as shown in Figure 5. However, the tensile forces acting on the tension leg increased significantly with the CD1 configuration, influenced by the distortion of the twin SFT models.

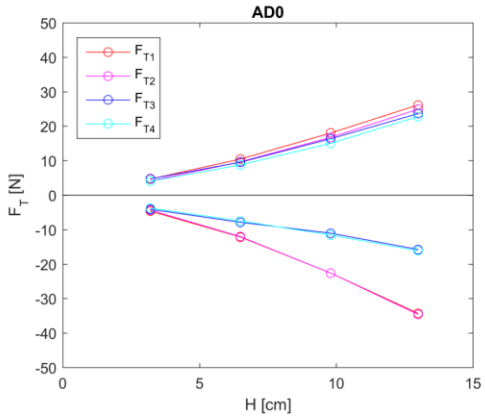

Figure 8. Maximum tensile forces acting on the tension legs of the twin SFT with the AD0 configuration (T = 1.3 s).

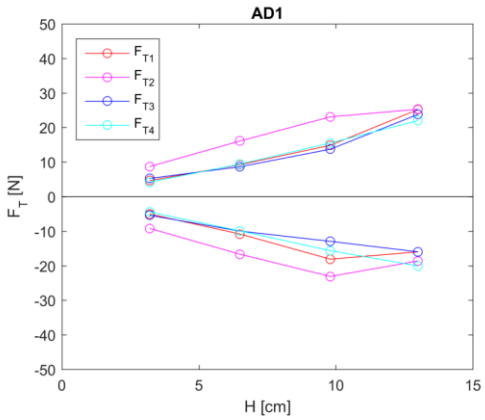

Figure 9. Maximum tensile forces acting on the tension legs of the twin SFT with the AD1 configuration (T = 1.3 s).

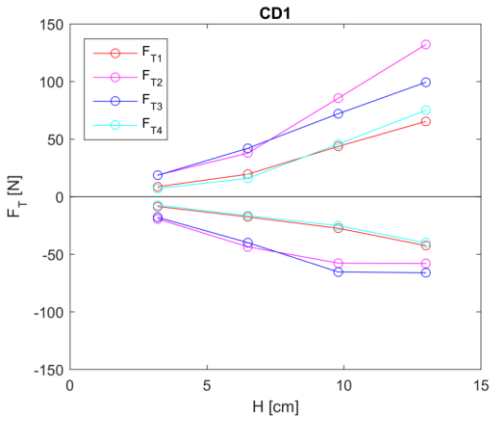

Figure 10. Maximum tensile forces acting on the tension legs of the twin SFT with the CD1 configuration (T = 1.3 s).

Figures 11 to 13 show the measurement results of the maximum dynamic pressure obtained from the eight pressure sensors that were attached to each SFT model when T = 1.3 s for the three different configurations. Overall, the measured pressure showed a linearly increasing trend with the wave height. Depending on the location of the sensors, the magnitudes of the pressures showed a significant difference. In the case of the AD0 configuration, the highest pressure was observed at the sensors p_1 and p_9 attached to the top surface of the first and second models, respectively. On the other hand, the lowest pressure was found at the sensors p_5 and p_{13} attached to the bottom surface of both models. However, the locations of the sensors showing the maximum and minimum pressures were different in the other two configurations, as shown in Figures 12 and 13. In addition, the maximum values of the first model were slightly higher than those of the second model in the AD0 and CD1 configurations, whereas the reverse trend was observed in the AD1 configuration. For other conditions of the wave period, similar trends as shown in Figures 11 to 13 were observed, although the magnitudes of pressures were different from one another.

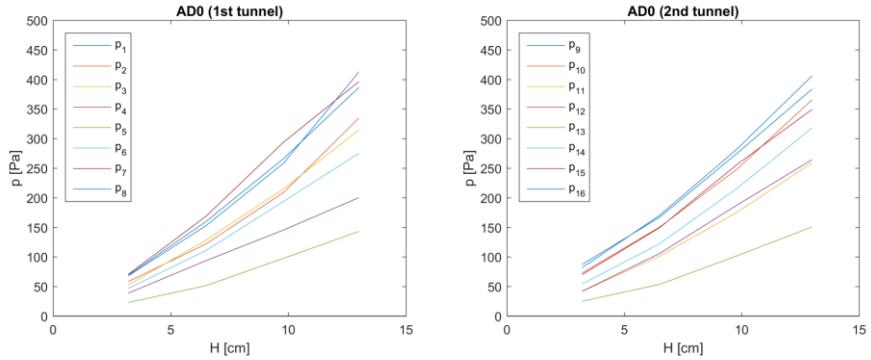

Figure 11. Maximum positive pressures on the SFT model with the AD0 configuration (T = 1.3 s).

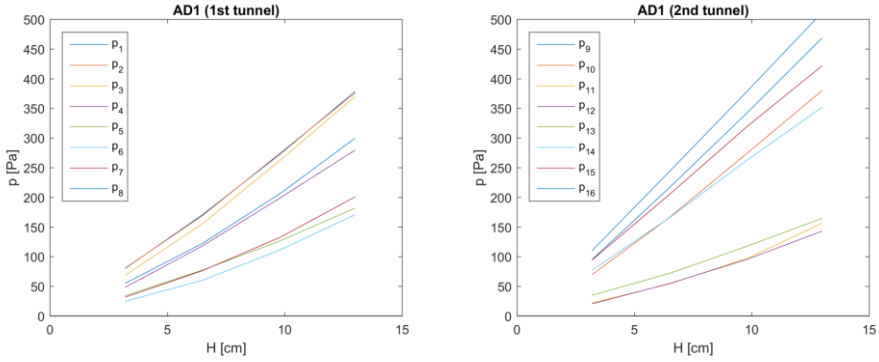

Figure 12. Maximum positive pressures on the SFT model with the AD1 configuration (T = 1.3 s).

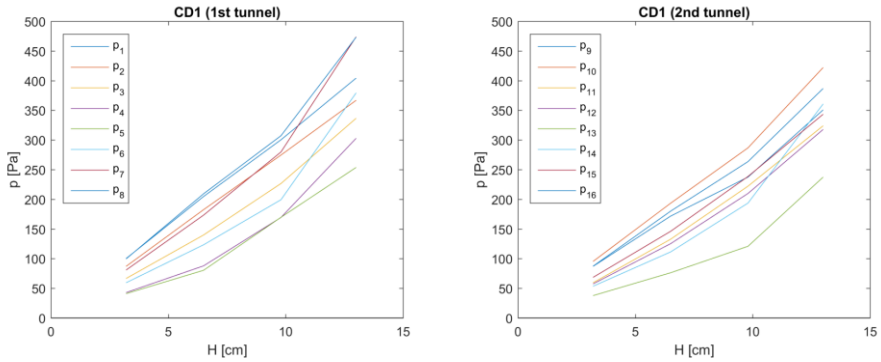

Figure 13. Maximum positive pressures on the SFT model with the AD1 configuration (T = 1.3 s).

4 CONCLUSIONS

This study carried out experiments to investigate the motions of a twin circular SFT and its hydrodynamic characteristics under wave loading. By analyzing the experimental data, we compared three different configurations of the twin SFT with respect to the motions of the two respective SFT models, the forces acting on the tension legs, and the pressures around the two tunnel bodies. In general, the magnitudes of the motions and the forces of SFT increased with an increase in the wave height and period. All the three configurations examined in this study showed no negligible displacements of the SFT models, indicating a lack of satisfaction with designs as a possible means of passage for transportation. Hence, further studies are being conducted to improve the design of the tension legs for the twin SFT, and the results of these studies are expected to be disclosed in the near future. In addition, the stiffness or elasticity of the tension legs may affect the structural response of the SFT under wave attack, the effect of which cannot be elucidated appropriately with the present experiment. A numerical simulation will be helpful for validating the experimental results and investigating the effects of parameters that are not well dealt with in the experiment.

ACKNOWLEDGEMENT

This research was supported by the KIOST (Korea Institute of Ocean Science and Technology) research program (project No. PE99424)

REFERENCES

Dong, M.-S., Miao, G,-P., Yong, L.-C., Niu, Z.-R., Pang, H.-P. and Hou, C.-Q., 2012. Effects of escape device for Submerge Floating Tunnel (SFT) on hydrodynamic loads applied to SFT, *J. Hydro. Ser. B*, 24, 4, 609-616.

Hong, Y. and Ge, F., 2010. Dynamic response and structural integrity of submerged floating tunnel due to hydrodynamic load and accidental load, *Proc. Engrg.*, 4, 35-50.

Jakobsen, B., 2010. Design of submerged floating tunnel operating under various conditions, *Proc. Engrg.*, 4, 71-79.

Kanie, S., Mikami, T. and Kakuta Y., 1997. Dynamic characteristics of submerged floating tunnels due to wave force, *Proc. JSCE*, 556, 159-168.

Kunish, H., 2010. Evaluation of wave force acting on submerged floating tunnels, *Proc. Engrg.* 4, 99-105.

Lu, W., Ge, F., Wang, L., Wu, X. and Hong, Y., 2011. On the slack phenomena and snap force in tethers of submerged floating tunnels under wave conditions, *Mar. Struct.*, 24, 358-376.

Society of submerged floating tunnel technology, 1997a. *Submerged floating tunnel - I. From planning to design and construction (in Japanese)*.

Society of submerged floating tunnel technology, 1997b. *Submerged floating tunnel - II. Case Study (in Japanese)*.